Performance and radiation tolerance of InAs/GaSb LWIR detectors based on CBIRD design

Alexander Soibel, David Z.-Y. Ting, Sir. B. Rafol, Arezou Khoshakhlagh, Anita Fisher, Sam. A. Keo, and Sarath D. Gunapala

Jet Propulsion Laboratory, California Institute of Technology, 4800 Oak Grove Dr., Pasadena, CA, 91109

ABSTRACT

We report our recent developments of antimonide based infrared photodetectors utilizing a complementary barrier infrared detector (CBIRD) design. The new generation of devices can operate close to zero bias with the same quantum efficiency as the initial design. 320x256 pixel long-wavelength infrared focal plane arrays utilizing optimized design have been demonstrated with 8.8 μm cutoff wavelength and noise equivalent differential temperature of 26 mK at operating temperature of 80 K for 300 K background and *f*/2 optics. As CBIRD detectors became valuable candidates for space-based instruments, question of their radiation tolerance became important. Here, we report our investigations of the proton irradiation effects on the photodetector performance.

Keywords: unipolar barrier, heterostructure, infrared, photodetector, superlattice

1. INTRODUCTION

The nearly lattice-matched InAs/GaSb/AlSb (antimonide) material system offers tremendous flexibility in realizing high-performance infrared detectors. Antimonide-based superlattice (SL) detectors[1] can be tailor-made to have cutoff wavelengths ranging from the short wave infrared (SWIR) to the very long wave infrared (VLWIR). These detectors are predicted to have suppressed Auger recombination rates[2,3] and low interband tunneling,[4,5] resulting in the suppressed dark currents. Moreover, the nearly lattice-matched antimonide material system, consisting of InAs, GaSb, AlSb and their alloys, allows for the construction of superlattice heterostructures. In particular, unipolar barriers, which blocks one carrier type without impeding the flow of the other, have been implemented in the design of SL photodetectors to realize complex heterodiodes with improved performance. Heterostructure superlattice detectors that make effective use of unipolar barriers have demonstrated strong reduction of generation-recombination (G-R) dark current due to Shockley-Read-Hall (SRH) processes. Despite relatively short lifetimes found in present day superlattice material, the higher absorber doping levels afforded by immunity to tunneling has led to reduced diffusion dark current. The dark current characteristics of type-II superlattice based single element LWIR detectors are now approaching that of the state-of-the-art MCT detector. However, noise measurements highlight the need for surface leakage suppression, which can be tackled by improved etching, passivation, and device design. The various aspects of type-II superlattice infrared detectors have been covered in detail in review articles by Fuchs *et al*. [6], Bürkle and Fuchs [7], Razeghi and Mohseni [8], and Ting *et al*. [9], as well as in the book by Rogalski [10]. In this paper, we discuss recent developments in the area of type-II superlattice based infrared detectors at the Jet Propulsion Laboratory (JPL).[11-20]

*Alexander.Soibel@jpl.nasa.gov; phone 818 393 0225; fax: 818 393 4540;

2. THE COMPLEMENTARY BARRIER INFRARED DETECTOR

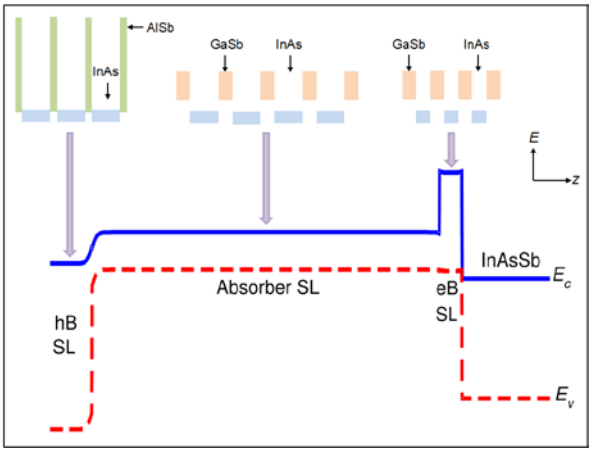

Figure 1. Calculated zero-bias energy band diagram of a complementary barrier infrared detector (CBIRD) structure, where a long-wave infrared InAs/GaSb superlattice absorber is surrounded by an InAs/AlSb superlattice hole-blocking (hB) unipolar barrier and a shorter period InAs/GaSb superlattice superlattice electron-blocking (eB) unipolar barrier.

The CBIRD design, consists of an InAs/GaSb absorber SL sandwiched between an InAs/AlSb unipolar hole barrier (hB) SL, and an InAs/GaSb unipolar electron barrier (eB) SL. Figure 1 shows calculated energy band diagrams of the CBIRD device. We expect the InAs/GaSb LWIR SL to have more favorable electron transport properties. Therefore the absorber superlattice is doped lightly p-type so that we have better minority carrier (electron) mobility. A full description of the device structure is published elsewhere.[11] The device structure was grown on GaSb (100) substrate by molecular beam epitaxy (MBE). Standard contact mode optical lithography was used to fabricated large-area (220×220 μm^2 in size) devices for dark current and responsivity measurements.

In the device reported in Reference 11, we observed that the photoresponse increases with bias from 0 to ~0.2 V, and then plateaus for bias greater than 0.2 V. The 77 K dark current density at 0.2 V is still quite low, with a value of ~1×10^{-5} A/cm^2. Arrhenius plot shows that at 0.2 V, the dark current is diffusion limited for device temperature above ~77K. Spectral response measured under 0.2 V applied bias at 77 K shows that the device has a 10 μm cutoff (defined by 50% peak responsivity), with a peak responsivity of 1.5 A/W. We calculated the shot-noise limited black-body D^*, where the noise spectrum is determined by the measured dark current and photocurrent integrated over the 8 μm to 10 μm spectral range (the overlap between the atmospheric window and the detector cutoff). Under 0.2 V, the detector reaches 300 K BLIP operation at 86 K with a black-body BLIP D^* value of 1.1×10^{11} cm-Hz$^{1/2}$/W for f/2 optics. For 300K background with 2π field of view, the device shows a BLIP temperature of 101 K with a black-body BLIP D^* value of 2.6×10^{10} cm-Hz$^{1/2}$/W. The device has a zero-bias dynamic resistance-area product of R_0A =14,000 ohm-cm^2 at 77 K. However, since the detector is expected to operate at a higher bias (~0.2 V), a more relevant quantities is the effective resistance-area product, given by $RA_{\text{eff}} = kT/qJ_d$. Under a 0.2 V bias, the RA_{eff} for this device is 670 ohm-cm^2 at 77 K.

Figure 2 compares the bias dependence of normalized QE of the first and current generation CBIRD devices. The initial devices required an applied bias of about 200 mV to operate the photodetectors, while the current devices can operate at zero bias and their spectral characteristics are bias independent. It was previously unknown whether the non-zero bias operation was an intrinsic property of CBIRD design resulting from utilization of unipolar barriers in the device architecture. The zero-bias operation of the current devices clearly demonstrates that, similar to the pn photodiode, the CBIRD design does not require extra turn-on bias. We associate the bias needed to operate the first generation of CBIRD devices with the formation of an unintended electron barrier near the hole-barrier-absorber interface, as discussed elsewhere [15].

Optical characterization tools are invaluable in the study of the material properties of CBIRD detectors. We have been investigating CBIRD devices using two different optical characterization techniques: photoluminescence (PL) and transmission spectroscopy. We find that the absorption quantum efficiency (QE), deduced from the transmission measurements, served as a good estimate of the upper limit of the external QE, and the PL peak position was shown to correlate well with the detector cut-off wavelength. In a comparison between the PL intensity and the dark current characteristics, a good correlation between a high PL intensity and low dark current was observed, showing that the PL intensity well reflects the material quality. Also, SRH processes were identified as the limiting factor of the minority carrier lifetime of the CBIRD material studied. More details of these optical characterization results can be found in Reference 12.

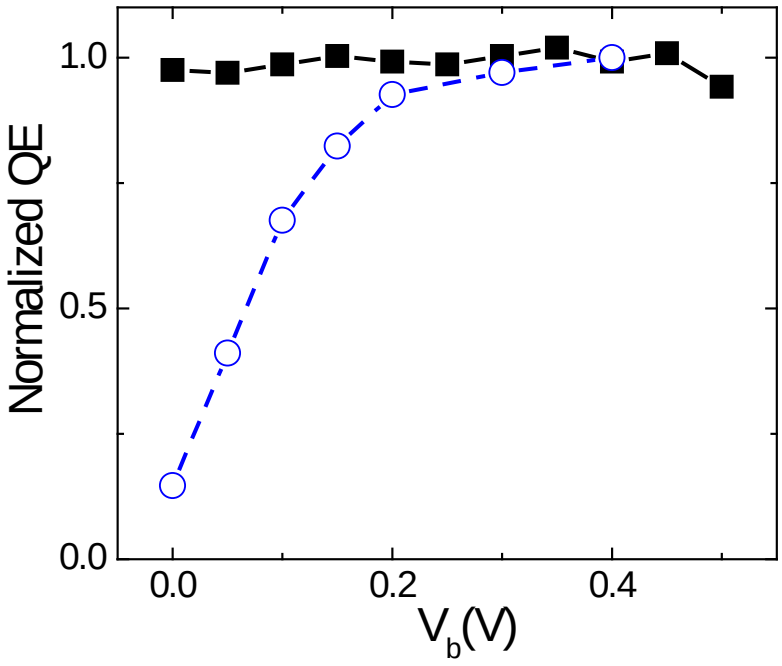

Figure 2. Bias dependence of normalized QE of the first (empty circle, blue) and current generation (filled square, black) of CBIRD devices.

We have also experimentally investigated the noise and gain of high-performance LWIR superlattice photodetectors. We compare the recently demonstrated SL heterodiode, which exhibits an electrical gain much larger than unity, with a SL photodetector without gain to show that the electrical gain in these devices originates from the device structure rather than from the superlattice absorber. We directly measure the noise spectra of high performance superlattice photodiodes, and demonstrated that intrinsically SL photodetectors do not exhibit 1/*f* noise. At the same time, our measurements clearly show that sidewall leakage current not only increases the shot noise by contributing to higher dark current but more importantly, it also introduces additional frequency dependent noise (potentially *1/f* noise), resulting in much higher noise in the detector. The 1/*f* noise has been extensively studied in p-n junctions. In particular, in MCT photodiodes, 1/*f* noise has been often associated with modulation of the surface generation currents induced by fluctuations of the surface potential. While the mechanisms of the surface leakage current in the Sb-based SL photodiodes are not completely understood yet, evidently the surfaces current can be a source of extraneous noise in these devices similar to MCT detectors. Since strong frequency-dependent noise can be generated by sidewall leakage current, it is important to fabricate the high performance SL detectors and focal plane array (FPA) using the technology that can minimize the mesa side-wall leakage current. One way to achieve this result is by development of reliable sidewall passivation that can suppress the leakage current and prevent the onset of frequency-dependent noise. More details of these noise and gain studies can be found in Reference 13.

We have also developed a dry-etch technique for pixel isolation for achieving low surface leakage for LWIR superlattice detectors. The surface leakage was reduced through the etching mechanism by minimizing the amount of differential etching and removing unwanted native oxides, byproducts, and contaminants on the sidewalls. The advantages to both chlorine-based and methane-based plasmas were exploited and combined to achieve over two orders of magnitude improvement in dark current compared to diodes etched with BCl_3/Ar. Each gas in $CH_4/H_2/BCl_3/Cl_2$/Ar etch governed its own unique role in minimizing surface leakage. CH4/H2 forms a thin polymer layer that serves as a passivant and protectant while sustaining near-vertical sidewalls and allowing for lower-temperature etches due to its volatility. BCl_3 effectively removes native oxides that contributes to the surface potential, and Cl_2 was added to increase the etch rate and prevent mask erosion. Effectively utilizing the proper gas ratios and etch parameters, differential etching was eliminated and thus avoided ripples in the sidewalls, a source for electrically active sites. This etch technique was proven to achieve dark currents as low as wet etching while significantly improving fill factor and uniformity. Near-vertical, smooth sidewalls with minimal dielectric mask erosion were achieved with good anisotropy resulting in more than three times higher fill factor. These performance enhancements allow small pixel size, large format LWIR FPAs to become more realizable. More details of the dry-etch technique can be found in Reference 14.

3. CBIRD FOCAL PLANE ARRAY DEVELOPMENT

The 320 x 256 pixel detector arrays with a 30 μm pixel pitch were fabricated by dry etching using a combination of gases: $CH_4/H_2/BCl_3/Cl_2$/Ar in an inductively coupled plasma.[17] Detector arrays were fully delineated, with etching into the bottom contact that was followed by Ohmic metal contact evaporation and a lift-off process. Next, small indium bumps were evaporated on top of the detector arrays. After indium evaporation and lift-off, wafers were diced to individual arrays. The PECs were mounted on chip carriers, bonded, and transferred to testing. The detector arrays were hybridized using a FC-300 flip-chip bonder with a FLIR/Indigo direct injection ISC0903 readout integrated circuit (ROIC) and then were backfilled with epoxy. Next, the substrate was completely removed by mechanical lapping followed by a dry etch process. The FPAs were mounted and wire-bonded to standard 84-pin ceramic leadless chip carriers (LCCs).

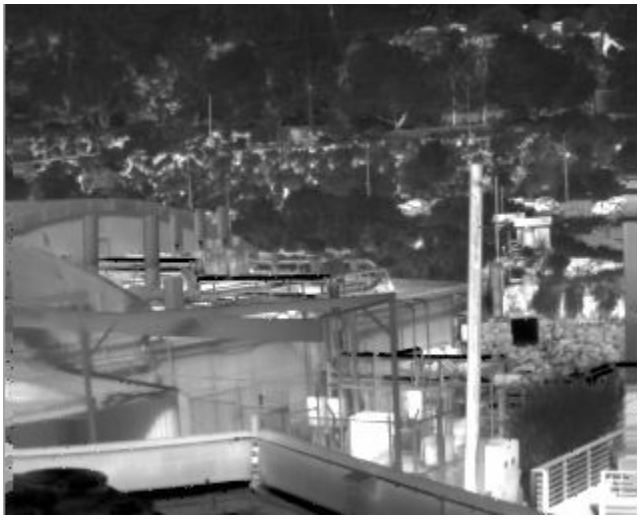

Figure 3. Outside images taken with the long-wavelength infrared n-CBIRD superlattice focal plane array. The FPA is operated at 78K with NEDT of 18.6 mK with f/2 optics at 300K background. This images show good quality reproduction of low and high spatial frequency.

The FPA was cooled down to 78K for data acquisition with general purpose SEIR test system. All measurements were done on the FPA directly. Figure 3 shows image of outside natural scenery taken with developed FPAs and 100 mm f/2 lens. The measured maximal QE is 54% is for double pass and cut-off wavelength is about 8.8μm. The operability of 97 % as defined as those pixels with reponsivity between 20 % and 150 % of the mean responsivity. The mean noise equivalent difference temperature (NEΔT) of 18.6 mK was measured for f/2 optics at 300K background.

4. RADIATION TOLERANCE STUDIES

As CBIRD superlattice detectors and focal plane arrays (FPAs) became valuable candidates for space-based instruments, question of their radiation tolerance became important. To address this question, we investigated the effect of the proton irradiation on the photodetector performance.[20]

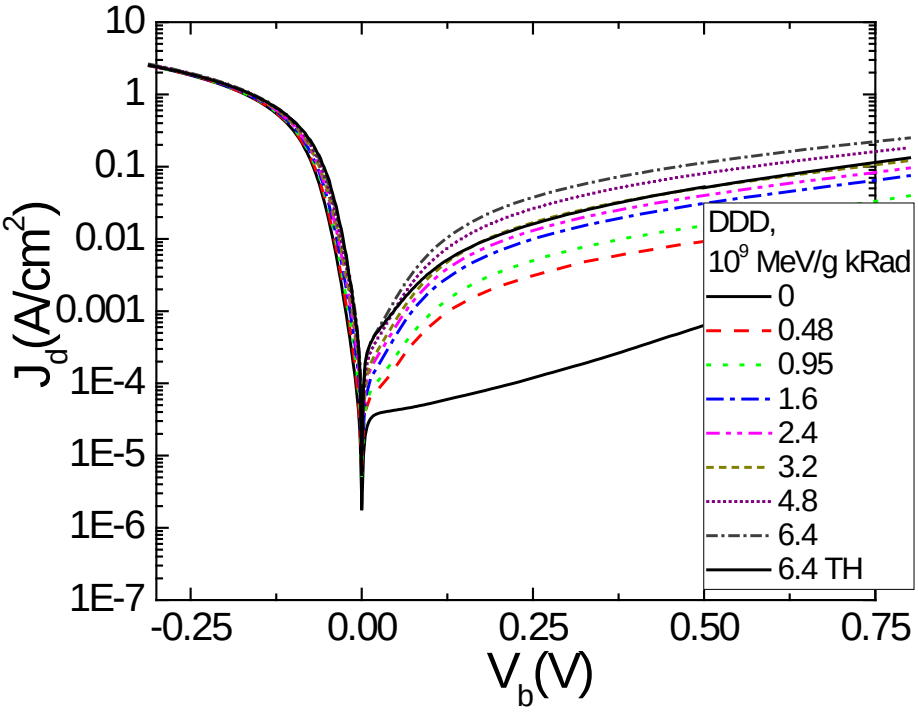

Figure 4. Dark current density of 150μm square single pixel photodiode operating at temperature T = 80K measured after the detector exposure to proton irradiation with total irradiation dose (TID) shown in the graph legend. The dark current measured after thermocycling is denoted as "200TH".

Devices used in this work utilize the CBIRD design described in detail in Ref. 11, 15. Detectors were loaded into IR Lab liquid nitrogen pour-fill dewar with a switchable cold shutter that enabled uninterrupted consecutive dark current and photocurrent measurements. The detectors were cooled down to 80K and tested with a moveable set-up that was later used during the radiation test. The 68MeV proton exposure was performed at the University of California, Davis, with isochronous cyclotron at Crocker Nuclear Laboratory. Detectors were kept unbiased at T = 80 K during irradiation and the time of each radiation session was set to about 15 min by adjusting the proton flux. The total ionizing dozes, TID, were 0, 15, 30, 50, 75, 100, 150 and 200 kRad, and the corresponding fluences were 1.4, 2.8, 4.8, 7.2, 9.6, 14.4 and 19.2 x10^{11} H+/cm^2. Dark current and photoresponse were tested prior to the irradiation and after each dose. After the full set of irradiations were completed, detectors were warmed to room temperature and kept at ambient conditions for several months. Then they were cooled down to T = 80K and re-tested with both portable and stationary systems.

Figure 4 shows the dark current density of 150μm square photodiode operating at T =80K for various TIDs. Dark current density of these devices increases with TID and the shape of $j(V)$ curves exhibits a pronounced change just after the first irradiation. The dark current density is j_d = 5x10^{-5} A/cm^2 at V_b = 0.1V at TID = 0 kRad and it increases by order

of magnitude to j_d = 6x10^{-4} A/cm^2 after the first irradiation with TID = 15 kRad. The dark current continues to increase linearly with TID (reaching j_d = 6x10^{-3} A/cm^2 at TID = 200 kRad. The change in the dark current with dose can be described, as $j_d = j_{d0}+K_{jd}\Phi p$, where K_{jd} is the dark damage factor and Φp is the proton irradiation fluence. Fit to data gives $K_{jd} \approx$ 2.2-3.5x10^{-15} (A/cm^2) /(H+/cm^2). Detector thermocycling resulted only in a small reduction of dark current to j_d = 4x10^{-3} A/cm^2, showing that the radiation damage is not annealed at room temperature and can be attributed to the displacement effects.

Figure 5 shows the dark current density of square 125, 150 and 250 μm photodiodes vs. perimeter/area ratio, P/A. Before the irradiation, there is no clear dark current dependence on the perimeter/area ratio and the two large devices have the largest dark current in this set. The situation changes after the irradiation when a linear dependence of the dark current on the perimeter/area is observed. We can extract the bulk dark current after the irradiation, j_{ba}, from the intersection of the linear fit curve with the axis. This gives $j_{ba} \approx$ 2x10^{-3} A/cm^2 which is significantly lower than the dark current measured for 150μm device after irradiation, $j \approx$6x10^{-3} A/cm^2 but is still much higher than the photodiode dark current before the irradiation, j_d = 5x10^{-5} A/cm^2. This indicates that the irradiation increases both bulk and surface dark currents, but the damage near the detector side wall has a larger effect on the dark current.

The maximal QE, $QE_{max} \approx 0.35$ was measured at λ = 7μm and the device cut-off wavelength, λ_c = 10.2μm, was found from the inflection point. We used a narrow bandpass filter centered at λ_B = 8.6μm to measure the detector photoresponse during the irradiation studies. Before the irradiation $QE_B \approx 0.24$ and QE_B decreases with radiation dose to $QE_B \approx 0.21$ at TID = 200 kRad. The QE decrease is small, less than 15% over the full range of TID. The detector thermocycling resulted only in a very minor increase of Quantum Efficiency to $QE_B \approx 0.22$.

In summary, we found that proton irradiation up to the total ionization dose 200kRad has only a minor effect on the spectral characteristics of LWIR InAs/GaSb superlattice photodiodes based on CBIRD design. At the same time, proton irradiation significantly increases dark current measured in these devices. This change in the dark current mechanism is attributed to the onset of the surface leakage current. It indicates that material damage close to the detector side walls increases the surface leakage current, which has a major contribution to the device degradation. Adequate passivation of the detector side wall or development of planar device geometry can potentially reduce the radiation damage and enable radiation hard InAs/GaSb superlattice detectors.

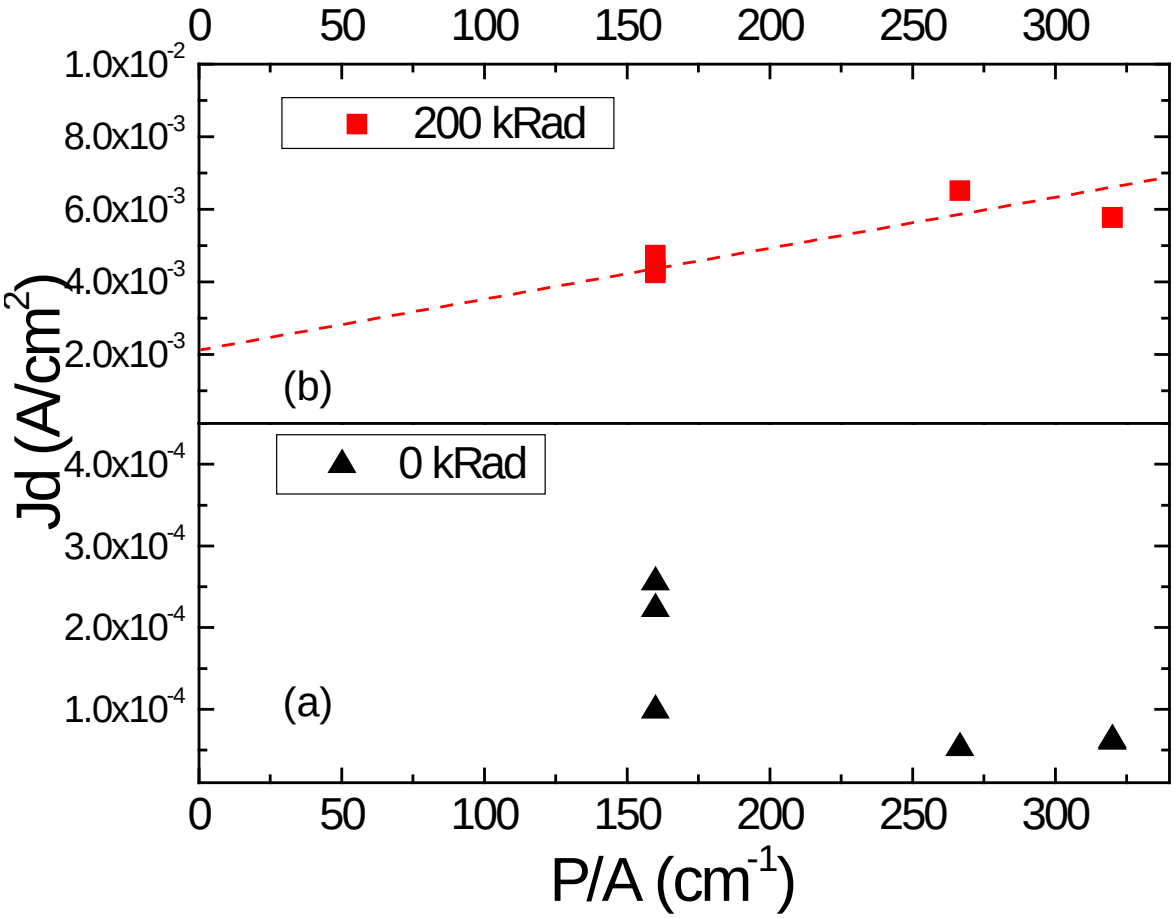

Figure 4. Dark current density measured at T = 80K and V_b = 0.1V vs. perimeter-to-area (P/A) ratio for TID = 0 kRad (panel a) and 200kRad (panel b). Red dashed line is a linear fit to data collected at TID=200kRad.

5. CONCLUSIONS

The antimonide material system is relatively robust and has the potential for good manufacturability. The versatility of the material system, with the availability of three different types of band offsets, provides great flexibility in device design. In the MWIR, the use of unipolar barriers in the nBn design has already seen success. In the LWIR, type-II InAs/Ga(In)Sb superlattices have been shown theoretically to have reduced Auger recombination and suppressed band-to-band tunneling. Suppressed tunneling allows for higher doping in the absorber, which has led to reduced diffusion dark current. Heterostructures such as those based on the CBIRD design have been used effectively to suppress G-R dark current. As a result, the dark current performance of antimonide superlattice based single element LWIR detectors are now approaching that of the state-of-the-art MCT detector, with sufficient performance for tactical applications and potential

for strategic applications. Reliable surface leakage current suppression methods, such as that based robust surface passivation, would be needed to improve radiation tolerance.

6. ACKNOWLEDGEMENT

The authors thank Dr. M. Tidrow, Dr. S. Bandara, and Dr. L. Zheng for encouragement and support. The research described in this publication was carried out at the Jet Propulsion Laboratory, California Institute of Technology, under a contract with the National Aeronautics and Space Administration. This work was sponsored by the Missile Defense Agency.

REFERENCES

[1] G. A. Sai-Halasz, R. Tsu, and L. Esaki, "A new semiconductor superlattice," *Appl. Phys. Lett.* **30**(12), 651-653 (1977).

[2] C. H. Grein, P. M. Young, and H. Ehrenreich, "Minority carrier lifetimes in ideal InGaSb/InAs superlattices," *Appl. Phys. Lett.* **61**(24), 2905 (1992).

[3] E. R. Youngsdale, J. R. Meyer, C. A. Hoffman, F. J. Bartoli, C. H. Grein, P. M. Young, H. Ehrenreich, R. H. Miles, and D. H. Chow, "Auger lifetime enhancement in InAs-$Ga_{1-x}In_xSb$ superlattices," *Appl. Phys. Lett.* **64**(23), 3160-3162 (1994).

[4] D. L. Smith and C. Mailhiot, "Proposal for strained type II superlattice infrared detectors," *Appl. Phys. Lett.* **34**(10), 663-665 (1987).

[5] D. L. Smith, T. C. McGill, and J. N. Schulman "Advantages of the HgTe-CdTe superlattice as an infrared detector material," *Appl. Phys. Lett.* **43**(2), 180-182 (1983).

[6] F. Fuchs, J. Wagner, J. Schmitz, N. Herres, and P. Koidl, "Growth and Characterization of InAs/AlSb/GaSb Heterostructures." in *Antimonide-related strained-layer heterostructures* (M. O. Manasreh, Ed.), pp. 191-232. Gordon Breach Science Publishers, Amsterdam (1997).

[7] L. Bürkle and F. Fuchs, "InAs/(GaIn)Sb superlattices: a promising material system for infrared detection" in *Handbook of Infrared Detection Technologies* (M. Henini and M. Razeghi, Ed.), pp. 159-189. Elsevier Science, Oxford (2002).

[8] L. Bürkle and F. Fuchs, "GaSb/InAs superlattices for infrared FPAs" in *Handbook of Infrared Detection Technologies* (M. Henini and M. Razeghi, Ed.), pp. 191-232. Elsevier Science, Oxford (2002).

[9] David Z.-Y. Ting, Alexander Soibel, Linda Höglund, Jean Nguyen, Cory J. Hill, Arezou Khoshakhlagh, and Sarath D. Gunapala, "Type-II Superlattice Infrared Detectors" in *Semiconductors and Semimetals*, Vol. 82, *Advances in Infrared Photodetectors* (S. Gunapala, D. Rhiger, and C. Jagadish, Ed.), Elsevier (2011).

[10] A. Rogalski, *Infrared Detectors*, CRC Press, Boca Raton (2011).

[11] D. Z.-Y. Ting, C. J. Hill, A. Soibel, S. A. Keo, J. M. Mumolo, J. Nguyen, and S. D. Gunapala, "A high-performance long wavelength superlattice complementary barrier infrared detector," *Appl. Phys. Lett.* **95**, 023508 (2009).

[12] Linda Höglund, Alexander Soibel, Cory J. Hill, David Z. Ting, Arezou Khoshakhlagh, Anna Liao, Sam Keo, Michael C. Lee, Jean Nguyen, Jason M. Mumolo, Sarath D. Gunapala, "Optical studies on antimonide superlattice infrared detector material", *Proc. SPIE* **7780**, 77800D (2010).

[13] Alexander Soibel, David Z.-Y. Ting, Cory J. Hill, Mike Lee, Jean Nguyen, Sam A. Keo, Jason M. Mumolo, and Sarath D. Gunapala, "Gain and noise of high-performance long wavelength superlattice infrared detectors", *Appl. Phy. Lett.* **96**(11), 111102 (2010).

[14] Jean Nguyen, Alexander Soibel, David Z.-Y. Ting, Cory J. Hill, Mike C. Lee, and Sarath D. Gunapala, "Low dark current long-wave infrared InAs/GaSb superlattice detectors", *Appl. Phy. Lett.***97**(5), 051108 (2010).

[15] D. Z. Ting, A. Soibel, J. Nguyen, L. Höglund, A. Khoshakhlagh, S. B. Rafol, S. A. Keo, A. Liao, J. M. Mumolo, J. K. Liu and S. D. Gunapala, "Type II superlattice barrier infrared detector," *Proc. SPIE*, vol. 8154, pp. 81540L0-12, 2011.

[16] Soibel, J. Nguyen, L. Höglund, C. Hill, D. Z. Ting, S. A. Keo, J. Mumolo, M. Lee, S. D. Gunapala, InAs/GaSb superlattice based long-wavelength infrared detectors: Growth, processing, and characterization; **Infrared Physics and Technology**, v 54, n 3, p 247-251, (2011)

[17] S. B. Rafol, A. Soibel, A. Khoshakhlagh, J. Nguyen, J. K. Liu, J. M. Mumolo, S. A. Keo, D. Z. Ting, Performance of a 1/4 VGA Format Long-Wavelength Infrared Antimonides Based Superlattice Focal Plane Array, IEEE J. Quant. Electr. 48, 878-884, (2012).

[18] Soibel, J. Nguyen, A. Khoshakhlagh, S. B. Rafol, L. Hoeglund, S. A. Keo, J. M. Mumolo, J. Liu, A. Liao, D. Z.-Y. Ting and S. D. Gunapala, Long wavelength infared superlattice detectors and FPAs based on CBIRD design, Phot. Tech. Lett. 25, 875-878, (2013).

[19] David Z. Ting; Alexander Soibel; Sam A. Keo; Sir B. Rafol; Jason M. Mumolo; John K. Liu; Cory J. Hill; Arezou Khoshakhlagh; Linda H öglund; Edward M. Luong; Sarath D. Gunapala. Development of quantum well, quantum dot, and type II superlattice infrared photodetectors J. Appl. Remote Sens. 8 (1), 084998 (February 19, 2014); doi: 10.1117/1.JRS.8.084998

[20] A. Soibel, Sir. B. Rafol, A. Khoshakhlagh, J. Nguyen, L. Hoglund, A. M. Fisher, S. A. Keo, D. Z.-Y. Ting and S. D. Gunapala, Proton radiation effect on performance of InAs/GaSb complementary barrier infrared detector, Appl. Phys. Lett. 107, 261102 (2015);